Search for Standard Model Higgs Boson Production in Association with a W Boson using a Neural Network Discriminant at CDF

(CDF Collaboration)

(Dated: December 19, 2008)

Abstract

We present a search for standard model Higgs boson production in association with a W boson in proton-antiproton collisions ($p\bar{p} \to W^{\pm}H \to \ell\nu b\bar{b}$) at a center of mass energy of 1.96 TeV. The search employs data collected with the CDF II detector that correspond to an integrated luminosity of approximately 1.9 fb^{-1}. We select events consistent with a signature of a single charged lepton ($e^{\pm}/\mu^{\pm}$), missing transverse energy, and two jets. Jets corresponding to bottom quarks are identified with a secondary vertex tagging method, a jet probability tagging method and a neural network filter. We use kinematic information in an artificial neural network to improve discrimination between signal and background. The observed number of events and the neural network output distributions are consistent with the standard model background expectations, and we set 95% confidence level upper limits on the production cross section times branching fraction ranging from 1.2 to 1.1 pb or 7.5 to 101.9 times the Standard Model expectation for Higgs boson masses from 110 to 150 GeV/c^2, respectively.

PACS numbers: 13.85.Rm, 14.80.Bn

I. INTRODUCTION

Standard electroweak theory predicts a single fundamental scalar particle, the Higgs boson, which arises as a result of spontaneous electroweak symmetry breaking [1]; however, the Higgs boson has not been directly observed by experiments. It is in fact the only fundamental standard model particle which has not been observed. The current experimental constraint on the Higgs boson mass, $m_H > 114.4\,\mathrm{GeV}/c^2$ at 95% confidence level (C.L.), comes from direct Higgs boson searches at LEP2 experiments [2]. Global fits to electroweak measurements and LEP2 experiments combined results exclude masses above $185\,\mathrm{GeV}/c^2$ at 95% CL [3].

At the Tevatron $p\bar{p}$ collider at Fermilab, the next-to-leading-order (NLO) Higgs boson production cross section prediction is about 10 times larger for gluon fusion than for WH associated production, and the cross section for WH is about twice that of ZH [4]. The Higgs boson decay branching fraction is dominated by $H \to b\bar{b}$ for $m_H < 135\,\mathrm{GeV}/c^2$ and by $H \to W^+W^-$ for $m_H > 135\,\mathrm{GeV}/c^2$ [5]. Background QCD $b\bar{b}$ production processes have cross sections at least four orders of magnitude greater than that of Higgs boson production [6], and this renders searches in the $gg \to H \to b\bar{b}$ channel unviable. However, requiring the leptonic decay of the associated W boson reduces the huge QCD background rate. As a result, $WH \to \ell\nu b\bar{b}$ is considered to be one of the most sensitive processes for low mass Higgs boson searches [1].

Searches for $WH \to \ell\nu b\bar{b}$ at $\sqrt{s} = 1.96\,\mathrm{TeV}$ have been most recently reported by CDF [7, 8] and D0 [9] using data corresponding to an integrated luminosity of 955 pb^{-1} and 440 pb^{-1}, respectively. In this paper, we present an update on the search for $WH \to \ell\nu b\bar{b}$ production at CDF using about 1.9 fb^{-1} of data and improved analysis techniques. To increase the acceptance for double b-tagged events, we introduce another b-tagging algorithm, jet probability b-tagging, which uses the impact parameter information of tracks inside jets. In addition we increase the signal acceptance by including the electrons going into the forward region of the detector and introduce a multivariate discriminant technique using a neural network (NN) to reduce large background contamination after event selection.

The paper is organized as follows. Section II describes the CDF II detector. The event selection criteria are explained in Sec. III. In Sec. IV the b-tagging algorithms with SECVTX, b-tagging filter, and jet probability are discussed in detail. Contributions from the standard

[1] In this paper, lepton (ℓ) denotes electron ($e^{\pm}$) or muon ($\mu^{\pm}$), and neutrino (ν) denotes electron neutrino (ν_e) or muon neutrino (ν_μ).

model (SM) background are calculated in Sec. V for various sources. In Sec. VI, signal acceptance and systematic uncertainties are estimated. The Neural Network discriminant technique is described in Sec. VII. The results and statistical interpretation of the results are presented in Sec. VIII. Finally, our conclusions are presented in Sec. IX.

II. CDF II DETECTOR

The CDF II detector geometry is described using a cylindrical coordinate system [10]. The z-axis follows the proton direction, and the polar angle θ is usually expressed through the pseudorapidity $\eta = -\ln(\tan(\theta/2))$. The detector is approximately symmetric in η and in the azimuthal angle ϕ. The transverse energy is defined as $E_T = E \sin\theta$, and the transverse momentum $p_T = p \sin\theta$.

Charged particles are tracked by a system of silicon microstrip detectors and a large open cell drift chamber in the region $|\eta| \leq 2.0$ and $|\eta| \leq 1.0$, respectively. The tracking detectors are immersed in a 1.4 T solenoidal magnetic field aligned coaxially with the incoming beams, allowing measurement of charged particle momentum transverse to the beamline (p_T).

The transverse momentum resolution is measured to be $\delta p_T/p_T \approx 0.1\% \cdot p_T(\mathrm{GeV})$ for the combined tracking system. The resolution on the track impact parameter (d_0), or distance from the beamline axis to the track at the track's closest approach in the transverse plane, is $\sigma(d_0) \approx 40\,\mu$m, of which about $30\,\mu$m is due to the transverse size of the Tevatron beam itself.

Outside of the tracking systems and the solenoid, segmented calorimeters with projective tower geometry are used to reconstruct electromagnetic showers and hadronic jets [11–13] over the pseudo-rapidity range $|\eta| < 3.6$. A transverse energy is measured in each calorimeter tower where the polar angle (θ) is calculated using the measured z position of the event vertex and the tower location.

Small contiguous groups of calorimeter towers with signals are identified and summed together into an energy cluster. Electron candidates are identified in the central electromagnetic calorimeter (CEM) or in the forward, known as the plug, electromagnetic calorimeter (PEM) as isolated, mostly electromagnetic clusters that match a track in the pseudorapidity range $|\eta| < 1.1$ and $|\eta| < 2.0$, respectively. The electron transverse energy is reconstructed from the electromagnetic cluster with a precision $\sigma(E_T)/E_T = 13.5\%/\sqrt{E_T/(\mathrm{GeV})} \oplus 2\%$

for central [11] and $\sigma(E_T)/E_T = 16.0\%/\sqrt{E_T/(\mathrm{GeV})} \oplus 2\%$ for plug. Jets are identified as a group of electromagnetic (EM) and hadronic calorimeter clusters (HAD) which fall within a cone of radius $\Delta R = \sqrt{\Delta\phi^2 + \Delta\eta^2} \leq 0.4$ units around a high-E_T seed cluster [14]. Jet energies are corrected for calorimeter non-linearity, losses in the gaps between towers and multiple primary interactions. The jet energy resolution is approximately $\sigma(E_T) = [0.1E_T/(\mathrm{GeV}) + 1.0]$ GeV [15].

For this analysis, muon candidates are detected in three separate subdetectors. After at least five interaction lengths in the calorimeter, the muons first encounter four layers of planar drift chambers (CMU), capable of detecting muons with $p_T > 1.4\,\mathrm{GeV/c}$ [16]. Four additional layers of planar drift chambers (CMP) behind another 60 cm of steel detect muons with $p_T > 2.8$ GeV/c [17]. These two systems cover the same central pseudorapidity region with $|\eta| \leq 0.6$. Muons that exit the calorimeters at $0.6 \leq |\eta| \leq 1.0$ are detected by the CMX system of four drift layers. Muon candidates are then identified as isolated tracks which extrapolate to line segments or "stubs" in one of the muon subdetectors. A track that is linked to both CMU and CMP stubs is called a CMUP muon.

The missing transverse energy ($\not\!\!E_T$) is a reconstructed quantity that is defined as the opposite of the vector sum of all calorimeter tower energy depositions projected on the transverse plane. It is often used as a measure of the sum of the transverse momenta of the particles that escape detection, most notably neutrinos. To be more readily interpretable as such, the raw $\not\!\!E_T$ vector is adjusted for corrected jet energies and for the energy deposition of any minimum ionizing high-p_T muons.

The CDF trigger system is a three-level filter, with tracking information available at the first level [18]. Events used in this analysis have all passed the high-energy electron or muon trigger selection. The first stage of the central electron trigger requires a track with $p_T > 8$ GeV/c pointing to a tower with $E_T > 8$ GeV and $E_{\mathrm{HAD}}/E_{\mathrm{EM}} < 0.125$. The plug electron (MET+PEM) trigger requires a tower with $E_T > 8$ GeV, $E_{\mathrm{HAD}}/E_{\mathrm{EM}} < 0.125$ and the missing transverse energy ($\not\!\!E_T$) > 15 GeV. The first stage of the muon trigger requires a track with $p_T > 4$ GeV/c (CMUP) or 8 GeV/c (CMX) pointing to a muon stub. A complete lepton reconstruction is performed online in the final trigger stage, where we require $E_T > 18\,\mathrm{GeV}$ for central electrons (CEM), $E_T > 18\,\mathrm{GeV}$ and $\not\!\!E_T > 20\,\mathrm{GeV}$ for MET+PEM and $p_T > 18\,\mathrm{GeV}/c$ for muons (CMUP,CMX).

III. EVENT SELECTION

The results presented here use data collected between February 2002 and May 2007. The data collected using the CEM, CMUP and MET+PEM triggers correspond to 1.92 ± 0.12 fb^{-1}, while the data from the CMX trigger corresponds to 1.88 ± 0.11 fb^{-1}.

The observable final state from the $WH \to \ell\nu b\bar{b}$ signal consists of two b-jets plus a lepton and missing transverse energy. The leptonic W decay in WH events yields the high-p_T lepton and large missing transverse energy due to the neutrino.

Events are considered as WH candidates only if they have exactly one high-p_T isolated lepton candidate [19], with $E_T > 20\,\text{GeV}$ for electrons or $p_T > 20\,\text{GeV}/c$ for muons. Because the lepton from a leptonic W decay is well-isolated from the rest of event, the cone of $\Delta R = 0.4$ surrounding the lepton must contain less less than 10% of the lepton energy. A primary event vertex position is calculated by fitting a subset of particle tracks that are consistent with having come from the beamline. The distance between this primary event vertex and the lepton track z_0 must be less than 5 cm to ensure the lepton and the jets come from the same hard interaction. Some leptonic Z decays would mimic the single-lepton signature if one of the leptons is unidentified. Events are therefore rejected if a second track with $p_T > 10\,\text{GeV}/c$ forms an invariant mass with the lepton that falls in the Z-boson mass window ($76 < m_{\ell X} < 106\,\text{GeV}/c^2$). The selected events are required to have $\not\!\!E_T$ greater than 20 GeV.

In the plug region, we also require a high-p_T isolated lepton candidate with $E_T > 20$ GeV, with the same selection criteria as for the central region. In addition, because the QCD contamination is higher in the forward region, we impose stricter criteria on the missing transverse energy, which improves the QCD rejection by a factor of 4 while keeping signal efficiency of 80%. We require that $MET_{sig} > 2$, $\not\!\!E_T > 25$ GeV and $\not\!\!E_T > 45$ GeV when the $\not\!\!E_T$ is pointing close to a jet, and large transverse mass of the reconstructed W, $M_T(W) > 20$ GeV/c^2. Here, MET_{sig} is defined as the ratio of $\not\!\!E_T$ to a weighted sum of factors correlated with mismeasurement, such as angles between the $\not\!\!E_T$ and the jet and amount of jet energy corrections, and $M_T(W)$ is defined as follows:

$$M_T(W) = \sqrt{2p_T^{lep}\not\!\!E_T - \boldsymbol{p}_T{}^{lep} \cdot \boldsymbol{\not\!\!E}_T}.$$

The WH signal includes two jets originating from $H \to b\bar{b}$ decays; these jets are expected to have large transverse energy. The jets are required to be in the pseudorapidity range

covered by the silicon detector so that secondary vertices from b decays can be reconstructed. Specifically, we require the jets satisfy $E_T > 20$ GeV and $|\eta| < 2.0$. The search for $WH \rightarrow \ell\nu b\bar{b}$ is performed in the sample of events with $W+$ exactly 2 jets; however, samples of events with W+1,3,$\geq$4 jets are used to cross-check the background modeling.

To increase the signal purity of the W+2-jet events, at least one jet must be b-tagged by the SECVTX algorithm. Three exclusive b-tagged event categories are considered. The first category (ST+ST) is for events where there are two SECVTX b-tagged jets. The second category (ST+JP) consists of events where only one of the jets is b-tagged by the SECVTX and the second jet is b-tagged by jet probability. The third category (ST with NN filter) contains events where only one of the jets is b-tagged by the SECVTX and also passes the neural network b-tagging filter.

IV. b JET IDENTIFICATION ALGORITHM

The b-quark has a relatively long lifetime, and B hadrons formed during the hadronization of the initial b quark can travel a significant distance before decaying into a collection of lighter hadrons. The jets containing b-quark decay can be reconstructed by identifying tracks significantly displaced from the $p\bar{p}$ interaction point (primary vertex).

Multijet final states have dominant contributions from QCD light flavor jet production, but the standard model Higgs boson decays predominantly to bottom quark pairs. Correctly identifying the b quark jets helps to remove most of the QCD background. In this analysis, we introduce some b-identification algorithms to optimize the selection of b-quark jets.

A. Secondary Vertex b-Tagging

The SECVTX b-tagging algorithm is applied to each jet in the event, using only the tracks which are within η-ϕ distance of $\Delta R = 0.4$ of the jet direction. Displaced tracks in jets are used for the SECVTX reconstruction and are distinguished by a large impact parameter significance ($|d_0/\sigma_{d_0}|$) where d_0 and σ_{d_0} are the impact parameter and the total uncertainty from tracking and beam position measurements. Secondary vertices are reconstructed with a two-pass approach which tests for high-quality vertices in the first pass and allows lower-quality vertices in the second pass. In pass 1, at least three tracks are required to pass

loose selection criteria ($p_T > 0.5\,\mathrm{GeV}/c$, $|d_0/\sigma_{d_0}| > 2.0$), and a secondary vertex is fit from the selected tracks. One of the tracks used in the reconstruction is required to have $p_T > 1.0\,\mathrm{GeV}/c$. If pass 1 fails, then a vertex is sought in pass 2 from at least two tracks satisfying tight selection criteria ($p_T > 1.0\,\mathrm{GeV}/c$, $|d_0/\sigma_{d_0}| > 3.5$ and one of the pass 2 tracks must have $p_T > 1.5\,\mathrm{GeV}/c$). If either pass is successful, the transverse distance (L_{xy}) from the primary vertex of the event is calculated along with the associated uncertainty. This uncertainty $\sigma_{L_{xy}}$ includes the uncertainty on the primary vertex position. Finally jets are tagged positively or negatively depending on the L_{xy} significance ($L_{xy}/\sigma_{L_{xy}}$):

$$L_{xy}/\sigma_{L_{xy}} \geq 7.5 \quad \text{(positive tag)} \tag{1}$$

$$L_{xy}/\sigma_{L_{xy}} \leq -7.5 \quad \text{(negative tag)} \tag{2}$$

These values have been tuned for optimum efficiency and purity in simulated b-jet samples from decays of top quarks. The energy spectrum for those jets is similar to the spectrum for b jets from decays of Higgs bosons.

The sign of L_{xy} indicates the position of the secondary vertex with respect to the primary vertex along the direction of the jet. If the angle between the jet axis and the vector pointing from the primary vertex to the secondary vertex is less than $\pi/2$, L_{xy} is positively defined; otherwise, it is negative. If L_{xy} is positive, the secondary vertex points towards the direction of the jet, as in true B hadron decays. For negative L_{xy} the secondary vertex points away from the jet; this may happen as a result of mismeasured tracks. In order to reject secondary vertices due to material interaction, the algorithm vetoes two-track vertices found between 1.2 and 1.5 cm from the center of the silicon detector (the inner radius of the beampipe and the outer radius of the innermost silicon layer being within this range). All vertices more than 2.5 cm from the center are rejected.

The negative tags are useful for evaluating the rate of false positive tags, which are identified as "mistags" in the background estimates. Mismeasurements are expected to occur randomly; therefore the L_{xy} distribution of fake tags is expected to be symmetric with respect to zero. Simulated events are used to correct a small asymmetry due to true long-lived particles in light flavor jets.

The efficiency for identifying a secondary vertex is different in the simulated and observed datasets. We measure an efficiency scale factor, which is defined as the ratio of the observed to the simulated efficiencies, to be 0.95 ± 0.04 in a sample of high-E_T jets enriched in b jets

by requiring a soft lepton ($p_T > 8\,\mathrm{GeV}/c$) from semileptonic heavy quark decays [20].

B. Neural Network b-Tagging Filter

The sample tagged by the SECVTX algorithm still has significant contamination from falsely-tagged light-flavor or gluon jets and the misidentification of c quarks as b-jets [21]. This search uses a multivariate neural network technique to improve the SECVTX tagging purity [7, 8].

The neural network used in this article employs the JETNET[22] package. The tagger is designed with two networks in series. The $b - l$ network is trained to separate b-jets from light-quark jets (l-jets), and the $b - c$ network is trained to separate b-jets from c-jets. Jets that pass a cut on both of the NN outputs are accepted by the tagger. These neural networks are trained and applied only to jets that are already tagged by the SECVTX algorithm. The current NN b-tagging is tuned to increase the purity of the SECVTX b-tagged jets, not to increase the tagging efficiency.

The neural networks take as input 16 variables that are chosen primarily because the b-quark jets have higher track multiplicity, larger invariant mass, longer lifetime and a harder fragmentation function than c- and l-quark jets. The track parameters and L_{xy} significance are good discriminators for b-jets. The sum of transverse momentum p_T^{vtx} and mass M_{vtx} of the tracks in association with the displaced vertex are useful variables for identifying l-jets; however c-jets have p_T spectra similar to b-jets. Pseudo-$c\tau$ ($L_{xy} \times M_{\mathrm{vtx}}/p_T^{\mathrm{vtx}}$), the vertex fit χ^2, and the track-based probability of a jet to come from the primary vertex are the best discriminators for b-jets.

The NN b-tagger is further validated by comparing the performance on a b-enriched sample of SECVTX tagged heavy-flavor jets from events with an electron candidate with $E_T > 8\,\mathrm{GeV}$ electron data and from the corresponding Monte Carlo sample. A good agreement is found in NN b-tagger performance between data and Monte Carlo [7, 8].

The output of the neural net is a value ranging from 0 and 1 that can be tuned to reject 65% of light-flavor jets and about 50% of the c jets while keeping 90% of b-jets which were tagged by SECVTX. The data-to-Monte-Carlo scale factor, measured from the electron sample, is 0.97 ± 0.02. Note that this is an additional scale factor with respect to the SECVTX efficiency scale factor because all of the jets under consideration have already been tagged

by SECVTX.

C. Jet Probability b-tagging

The jet probability b-tagging algorithm distinguishes itself by employing the signed impact parameters, and their uncertainties, of tracks in jets and calculates the probability that the jet was produced at a position consistent with the primary vertex. The sign of impact parameter is defined according to the angle ϕ between the jet axis and the direction to the track's closest point of approach with respect to the primary vertex. The sign is positive (negative) if $\cos\phi > 0 (< 0)$. A feature of this algorithm is that the b-tagging is performed using a continuous variable instead of a discrete object like a reconstructed secondary vertex.

For a light-quark jet, most particles should originate from the primary vertex. Due to the finite tracking resolution, these tracks are reconstructed with a non-zero impact parameter and have an equal probability to be either positive or negative signed. Since a long lived particle will travel some distance along the jet direction before decaying, its decay products will preferentially have positive signed impact parameters.

To calculate the jet probability value, the tracking resolution can be extracted from the inclusive jets data by fitting the negative side of the signed impact parameter distribution obtained for prompt jets. Tracks are sorted into different categories (η, p_T of tracks, and quality of silicon detector hits) to parametrize their properties. To minimize the contribution from badly measured tracks with large reconstructed impact parameters, the distribution of a related quantity, the signed impact parameter significance S_{d_0} (ratio of the signed impact parameter to its uncertainty) is parametrized at each track category. The impact parameter significance for each track is required to satisfy the quality criteria of $p_T > 0.5\text{GeV}/c$ and a minimum number of hits in the tracking detector .

The resolution function is used to determine the track probability, which should be flat between 0 and 1 for tracks with a negative signed impact parameter. For the tracks originating from long-lived particles with large positive signed impact parameter, the track probability has a peak near zero.

To calculate jet probability, at least two tracks with positive impact parameter are required as the taggable condition. By definition, the jet probability distribution should be flat for jets having only prompt tracks. Tracks with a negative impact parameter are used

to define a negative P_{jet}, which is used to check the algorithm and to estimate the misidentification rate. We choose an operation point whereby the fake rate becomes about 5%. At this point, the b-tagging efficiency is about 60%. The difference between the simulated and observed data is taken into account as a scale factor. We measure the scale factor to be 0.85±0.07 in a sample of high-E_T jets enriched in b jets by requiring a soft lepton from semileptonic heavy flavor decay. A more detailed description of the scale factor estimation is given in Ref. [23].

V. BACKGROUND

The final state signature of $WH \to \ell\nu b\bar{b}$ production can be mimicked by other processes. The dominant background processes are W+jets production, $t\bar{t}$ production, and non-W QCD multijet production. Several electroweak production processes also contribute but with smaller rates. In the following subsections the contribution from each background source is discussed in detail. These background estimations are based on the same strategies used in the previous analysis [7, 8]. A summary of the background estimate can be found in Sec. VIII.

A. Non-W QCD Multijet

Events from QCD multijet production sometimes mimic the W-boson signature by producing fake leptons or fake $\not\!\!E_T$. Non-W leptons are reconstructed when a jet passes the lepton selection criteria or a heavy-flavor jet produces leptons via semileptonic decay. Non-W $\not\!\!E_T$ can result from mismeasurements of energy or semileptonic decays of heavy-flavor quarks. Since the $\not\!\!E_T$ mismeasurement is usually not well modeled in detector simulation, we estimate the contribution of non-W events directly from the data sample before b-tagging is applied, known as the pretag sample.

Generally, the bulk of non-W events are characterized by a non-isolated lepton and small $\not\!\!E_T$. Lepton isolation I is defined as the ratio of calorimeter energy inside a cone of $\Delta R = 0.4$ about the lepton to the lepton energy itself. The quantity I is small if the lepton is well-isolated from the rest of the event, as typified by a true leptonic W decay. This feature is used to extrapolate the expected non-W contribution into our signal region, namely, small

I and large $\not\!\!E_T$. In extracting the non-W background contribution from data, we make the following two assumptions: lepton isolation and $\not\!\!E_T$ are uncorrelated in non-W events, and the b-tagging rate is not dependent on $\not\!\!E_T$ in non-W events. The level at which these assumptions are justified determines the assigned uncertainty. The contributions from $t\bar{t}$ and W+jets events are subtracted according to the calculated cross sections for those processes.

To validate the method and estimate the relevant systematic uncertainties, we vary the boundaries of signal and background regions. The observed deviations imply a 25% systematic uncertainty in the non-W background yield, assigned conservatively for both the pretag and tagged estimates.

A non-W rejection factor associated with the neural network b-tagging filter is measured from data in the background region ($I > 0.2$ and $\not\!\!E_T$ >20 GeV), which has event kinematics similar to non-W events in the signal region because lepton isolation is the only difference between the two regions. The non-W estimate calculated before applying NN b-tagging is scaled by this NN rejection factor; this assumes the NN filter is uncorrelated with the isolation.

The non-W estimate for events with at least two b-tags is obtained by measuring the ratio of the number of events with at least one b-tag to the number with at least two b-tags in the background region and applying the ratio to the estimate of tagged non-W events in the signal region.

For the plug region, the MET+PEM trigger is used, which means the above method is not valid, because of the $\not\!\!E_T$ trigger bias. The $\not\!\!E_T$ distribution shape difference between non-W background and other backgrounds is therefore used instead to measure the amount of non-W background. To model the non-W shape, the control samples with electron candidates which failed at least two of our standard lepton identification criteria are used. We perform a likelihood fit for observed data using the non-W template and other background templates.

B. Mistagged Jets

The rate at which SECVTX falsely tags light-flavor jets is derived from inclusive jet samples in varying bins of η, number of vertices, jet E_T, track multiplicity, z position of primary vertex and total event E_T scalar sum. Tag rate probabilities are summed for all of the taggable jets in the event (jets with at least two tracks well measured in the silicon detector).

Since the double-mistag rate is small, this sum is a good approximation of the single-tag event rate. Negative mistags are defined as tags with unphysical negative decay length due to finite tracking resolution, which assumed to be a good estimate of falsely tagged jets, independent to first order of heavy flavor content in the generic jet sample. The positive mistag rate can be obtained from the negative mistags with an additional correction factor, reflecting an enhancement of positive mistags due to light-flavor secondary vertices and material interactions in the silicon detectors. This factor is measured in inclusive jet sample by fitting the asymmetry in the vertex mass distribution of positive tags over negative tags [24]. The systematic uncertainty on the rate is largely due to self-consistency in the parametrization as applied to the generic jet sample. The mistag rate per jet is applied to events in the W+jets sample. The total estimate is corrected for the non-W QCD fraction and also the top quark contributions to the pretag sample. To estimate the mistag contribution in NN-tagged events, we apply the light flavor rejection power of the NN filter 0.35 ± 0.05 as measured using light-flavor jets from various data and simulated samples. To estimate the mistag contribution in double tagged events, we apply the mistag rate to all untagged jets in W + 1 b-tagged jet events. In this method, the mistag contribution is estimated due to a case of one real b-tag + one mistag and a double mistag case in which both b-tagged jet are not real.

For jet probability b-tagging, the mistag rate is derived from inclusive jet samples in varying bins of η, z position of the primary vertex, jet E_T, track multiplicity, number of vertices and total event E_T scalar sum. The mistag rate probabilities are derived and applied in the same way as for the SECVTX tag.

C. W+Heavy Flavor

The $Wb\bar{b}$, $Wc\bar{c}$, and Wc states are major background sources of secondary vertex tags. Large theoretical uncertainties exist for the overall normalization because current Monte Carlo event generators can generate W+heavy-flavor events only to leading order. Consequently, rates for these processes are normalized to data. The contribution from true heavy-flavor production in W+jet events is determined from measurements of the heavy-flavor event fraction in W+jet events and the b-tagging efficiency for those events, as explained below.

Jet Multiplicity	1 jet	2 jets	3 jets	≥ 4 jets
$Wb\bar{b}$ (1B) (%)	1.0 ± 0.4	2.0 ± 0.8	3.4 ± 1.4	4.6 ± 2.0
$Wb\bar{b}$ (2B) (%)	-	1.3 ± 0.6	2.5 ± 1.0	3.1 ± 1.8
$Wc\bar{c}$ (1C) (%)	7.7 ± 2.4	12.2 ± 4.5	16.4 ± 5.3	18.6 ± 6.9
$Wc\bar{c}$ (2C) (%)	-	2.0 ± 0.8	4.6 ± 1.8	8.4 ± 3.4

TABLE I: The heavy-flavor fractions, given in percent, for the W + jets sample where $1B$, $2B$ refer to number of taggable b-jets in the events, with $1C$, $2C$ for charm jets. The results from ALPGEN Monte Carlo have been scaled by the data-derived calibration factor of 1.4 ± 0.4.

The fraction of W+jets events produced with heavy-flavor jets has been studied extensively using an ALPGEN + PYTHIA combination of Monte Carlo simulations [25, 26]. Calculations of the heavy-flavor fraction in ALPGEN have been calibrated using a jet data sample, and measurements indicate a scaling factor of 1.4 ± 0.4 is necessary to make the heavy-flavor production in Monte Carlo match the production in W+1jet events. The final results obtained for heavy-flavor fractions are shown in Table I.

For the tagged W+heavy flavor background estimate, the heavy-flavor fractions and tagging rates given in Tables I and II are multiplied by the number of pretag W+jets candidate events in data, after correction for the contribution of non-W and $t\bar{t}$ events to the pretag sample. The W+ heavy flavor background contribution is obtained by the following relation:

$$N_{W+\mathrm{HF}} = f_{\mathrm{HF}} \cdot \epsilon_{\mathrm{tag}} \cdot [N_{\mathrm{pretag}} \cdot (1 - f_{\mathrm{non}-W}) - N_{\mathrm{TOP}} - N_{\mathrm{EWK}}] \,, \tag{3}$$

where f_{HF} is the heavy-flavor fraction, ϵ_{tag} is the tagging efficiency, N_{TOP} is the expected number of $t\bar{t}$ and single top events, and N_{EWK} is the expected number of WW, WZ, ZZ and Z boson events.

D. Top and Electroweak Backgrounds

Production of both single top quark and top-quark pairs contribute to the tagged lepton+jets sample. Several electroweak boson production processes also contribute. WW pairs can decay to a lepton, neutrino as missing energy, and two jets, one of which may be charm. WZ events can decay to the signal $Wb\bar{b}$ or $Wc\bar{c}$ final state. Finally, $Z \to \tau^+\tau^-$

Jet Multiplicity	1 jet	2 jets	3 jets	≥ 4 jets
1 SECVTX and NN b-tag (%)				
$Wb\bar{b}$ (1B)	27.5 ± 1.5	28.1 ± 1.3	26.7 ± 1.4	26.9 ± 3.7
$Wb\bar{b}$ (2B)	-	26.2 ± 1.2	24.1 ± 1.2	22.6 ± 1.3
$Wc\bar{c}$ (1C)	4.2 ± 0.2	4.6 ± 0.3	4.9 ± 0.3	5.2 ± 0.7
$Wc\bar{c}$ (2C)	-	6.3 ± 0.4	6.6 ± 0.4	6.9 ± 0.6
≥ 2 SECVTX b-tag (%)				
$Wb\bar{b}$ (2B)	-	16 ± 2	19 ± 2	19 ± 3
$Wc\bar{c}$ (2C)	-	1 ± 0	2 ± 0	2 ± 1
1 SECVTX + Jet Probability b-tag (%)				
$Wb\bar{b}$ (2B)	-	10.1 ± 1.2	11.1 ± 1.3	12.4 ± 1.5
$Wc\bar{c}$ (2C)	-	1.6 ± 0.2	2.3 ± 0.3	3.2 ± 0.4

TABLE II: The b-tagging efficiencies in percent for various b-tagging strategies on individual W+heavy-flavor processes. Categories $1B$, $2B$ refer to number of taggable b-jets in the events, with similar categories for charm jets. Those numbers include the effect of the data-to-Monte Carlo scale factors.

events can have one leptonic τ decay and one hadronic decay. The leptonic τ decay gives rise to a lepton + missing transverse energy, while the hadronic decay yields a narrow jet of hadrons with a non-zero lifetime.

The normalization of the diboson and single top backgrounds are based on the theoretical cross sections listed in Table III, the luminosity, and the acceptance and b-tagging efficiency derived from Monte Carlo events [19, 27–29]. The acceptance is corrected for lepton identification, trigger efficiencies, and the z vertex cut. The tagging efficiency is always corrected by the b-tagging scale factor.

VI. HIGGS BOSON SIGNAL ACCEPTANCE

The kinematics of the SM $WH \rightarrow \ell\nu b\bar{b}$ process are well defined, and events can be simulated accurately by Monte Carlo generators. PYTHIA is used to generate the signal samples [30]. Only Higgs boson masses between 110 and 150 GeV/c^2 are considered because

Background	Theoretical Cross Sections
WW	12.40 ± 0.80 pb
WZ	3.96 ± 0.06 pb
ZZ	1.58 ± 0.02 pb
Single top s-channel	0.88 ± 0.11 pb
Single top t-channel	1.98 ± 0.25 pb
$Z \to \tau^+\tau^-$	265 ± 30.0 pb
$t\bar{t}$	$6.7^{+0.7}_{-0.9}$ pb

TABLE III: Theoretical cross sections and uncertainties for the electroweak and single top backgrounds, along with the theoretical cross section for $t\bar{t}$ at $m_t = 175\,\mathrm{GeV}/c^2$. The cross section of $Z^0 \to \tau^+\tau^-$ is obtained in the dilepton mass range $m_{\tau\tau} > 30\,\mathrm{GeV}/c^2$ together with a k-factor (NLO/LO) of 1.4.

this is the mass region for which the decay $H \to b\bar{b}$ dominates. The number of expected $WH \to \ell\nu b\bar{b}$ events N is given by

$$N = \epsilon \cdot \int \mathcal{L}dt \cdot \sigma(p\bar{p} \to WH) \cdot \mathcal{B}(H \to b\bar{b}), \tag{4}$$

where ϵ, $\int \mathcal{L}dt$, $\sigma(p\bar{p} \to WH)$, and $\mathcal{B}(H \to b\bar{b})$ are the event detection acceptance, integrated luminosity, production cross section, and branching fraction, respectively. The production cross section and branching fraction are calculated to NLO precision [5]. The acceptance ϵ is broken down into the following factors:

$$\epsilon = \sum_{\ell=e,\mu,\tau} \left(\epsilon_{z_0} \cdot \epsilon_{\mathrm{trigger}} \cdot \epsilon_{\mathrm{lepton\ ID}} \cdot \epsilon_{b\mathrm{tag}} \cdot \epsilon_{\mathrm{kinematics}} \cdot \mathcal{B}(W \to \ell\nu)\right), \tag{5}$$

where ϵ_{z_0}, $\epsilon_{\mathrm{trigger}}$, $\epsilon_{\mathrm{lepton\ ID}}$, $\epsilon_{b\mathrm{tag}}$, and $\epsilon_{\mathrm{kinematics}}$ are efficiencies defined in sequence to meet the requirements of primary vertex, trigger, lepton identification, b-tagging, and event selection criteria. The major sources of inefficiency are the lepton identification, jet kinematics, and b-tagging factors; each is a factor between 0.3 and 0.45. The factor of ϵ_{z_0} is obtained using the vertex distribution from the minimum bias data, $\epsilon_{trigger}$ is measured using a clean $W \to l\nu$ data sample, obtained from different triggers after applying more stringent offline cuts, and $\epsilon_{\mathrm{lepton\ ID}}$ is calculated using $Z \to ll$ observed data and Monte Carlo samples. $\epsilon_{b\mathrm{tag}}$ is measured in a b-enriched sample from semileptonic heavy flavor decay. The total signal

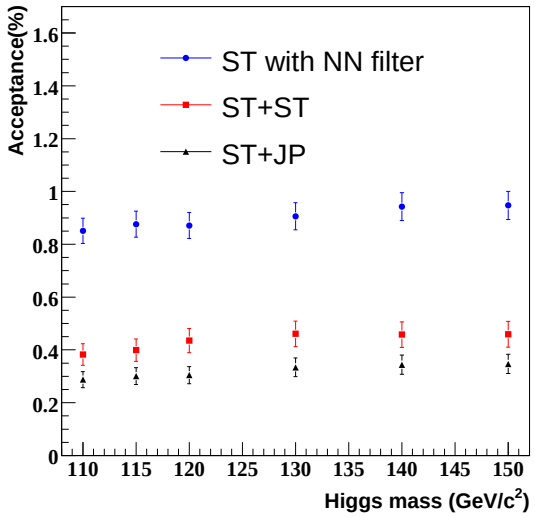

FIG. 1: The acceptance summary for the process $WH \to \ell\nu b\bar{b}$ in W+2jet bin for the selected b-tagging strategies as a function of Higgs boson mass.

b-tagging category	110 GeV	115 GeV	120 GeV	130 GeV	140 GeV	150 GeV
Pretag	9.41±0.61	7.92±0.52	6.35±0.41	3.99±0.26	2.02±0.13	0.78±0.05
ST with NN filter	2.63±0.22	2.20±0.18	1.70±0.14	1.08±0.09	0.55±0.05	0.21±0.02
ST+ST	1.18±0.14	1.00±0.12	0.85±0.10	0.55±0.07	0.27±0.03	0.10±0.01
ST+JP	0.89±0.11	0.76±0.09	0.60±0.07	0.40±0.05	0.20±0.02	0.08±0.01

TABLE IV: Expected number of $WH \to \ell\nu b\bar{b}$ signal events with systematic uncertainties for the selected b-tagging options.

acceptances are shown in Fig. 1 for the selected b-tagging options as a function of Higgs boson mass. The plug electron increases the overall acceptance by 10%.

The expected number of signal events is estimated by Eq. 4 at each Higgs boson mass point. The expectations for the selected b-tagging strategies are shown in Table IV.

The total systematic uncertainty on the acceptance stems from the jet energy scale, initial and final state radiation, lepton identification, trigger efficiencies, and b-tagging scale factor. A 2% uncertainty on the lepton identification efficiency is assigned for each lepton type (CEM electron, plug electron, CMUP and CMX muon), based on studies of Z boson events.

b-tagging category	LeptonID	Trigger	ISR/FSR	JES	PDF	b-tagging	Total
ST with NN filter	$\sim 2\%$	$< 1\%$	2.9%	2.3%	1.2%	3.5%	5.6%
ST+ST	$\sim 2\%$	$< 1\%$	5.2%	2.5%	2.1%	8.4%	10.6%
ST+JP	$\sim 2\%$	$< 1\%$	4.0%	2.8%	1.5%	9.1%	10.5%

TABLE V: Systematic uncertainties for the selected b-tagging requirements.

For each of the high p_T lepton triggers, a 1% uncertainty is measured from backup trigger paths or Z boson events.

The initial and final state radiation systematic uncertainties are estimated by changing the parameters related to ISR and FSR from nominal values to half or double the nominal [31]. The difference from the nominal acceptance is taken as the systematic uncertainty. The uncertainty in the incoming partons energies relies on the eigenvectors provided in the PDF fits. An NLO version of the PDFs, CTEQ6M, provides a 90% confidence interval of each eigenvector [32]. The nominal PDF value is reweighted to the 90% confidence level value, and the corresponding reweighted acceptance is computed. The differences between nominal and reweighted acceptances are added in quadrature, and the total is assigned as the systematic uncertainty [20].

The uncertainty on the jet energy scale (JES) [15] is calculated by shifting jet energies in WH Monte Carlo samples by $\pm 1\sigma$. The deviation from the nominal acceptance is taken as the systematic uncertainty. The systematic uncertainty on the b-tagging efficiency is based on the scale factor uncertainty discussed in Sec. IV A and IV C. When NN b-tagging filter is applied, the scale factor uncertainty is added to that of SECVTX in quadrature. The total systematic uncertainties for the selected b-tagging options are summarized in Table V.

VII. NEURAL NETWORK DISCRIMINANT

To improve further the signal to background discrimination after event selection, we employ an artificial neural network [22] trained on a variety of kinematic variables to distinguish the W+Higgs events from backgrounds.

We train the neural network on the samples of simulated events using a mixture of 50% signal with $m_h = 120$ GeV/c^2 and 50% of backgrounds. The background composition

is chosen to have equal amount of $Wb\bar{b}$, $t\bar{t}$, and single top, which provides a maximum sensitivity over a wide range of input conditions.

To optimize the neural network structure, we use an iterative procedure to determine the configuration that best discriminates signal from the background, and uses a minimal number of input discriminants. This is done by first determining the best one-variable network from a list of 76 possible variables, based on the kinematic distributions of the two jets, lepton, and $\not\!\!E_T$ in the events (including correlations between these objects). The optimization algorithm keeps this variable as an input and then loops over all other variables to determine the best two-variable network. The best N-variable network is finally selected once the N+1-variable network shows less than 0.5 percent improvement. The criteria for comparing networks is the testing error defined by how often a NN with a given configuration incorrectly classifies signal and background events.

We used the same structure of input variables to train separate neural networks for Higgs masses of 110, 115, 120, 130, 140, and 150 GeV/c^2. Re-training networks with different signal masses keep the neural network sensitivity almost constant as a function of the Higgs mass.

Our neural network configuration has 6 input variables, 11 hidden nodes, and 1 output node. The 6 optimal inputs are follows.

M_{jj+}**:** the invariant mass calculated from the two jets. Furthermore, if there are additional loose jets present ($E_T > 12$ GeV and $|\eta| < 2.4$), the loose jet that is closest to one of the two jets is included in this invariant mass calculation, if the separation between that loose jet and one of the jets is $\Delta R < 0.9$.

$\sum E_T$**(Loose Jets):** the scalar sum of transverse energy of the loose jets .

p_T **Imbalance:** the difference between the scalar sum of the transverse momenta of all measured objects and the $\not\!\!E_T$. Specifically, it is calculated as $P_T(jet_1) + P_T(jet_2) + P_T(lep) - \not\!\!E_T$.

$M_{l\nu j}^{min}$**:** the invariant mass of the lepton, $\not\!\!E_T$, and one of the two jets, where the jet is chosen to give the minimum invariant mass. For this quantity, the p_z component of the neutrino is ignored.

ΔR(**lepton-**ν_{max}**):** the ΔR separation between the lepton and the neutrino, where the p_z of the neutrino is taken by choosing the solutions from the quadratic equations for the W mass (80.42 GeV/c^2) constraint with the largest $|p_z|$.

$P_T(W+H)$**:** the total transverse momentum of the W plus two jets system, $P_T(l\vec{ep} + \vec{\nu} + j\vec{et}_1 + j\vec{et}_2)$.

All distributions are further checked and confirms that the data are well modeled by the Monte Carlo events in both pretag and tag samples. The output of the neural network is a value from 0 and 1 that will provide a discrimination between the signal and backgrounds.

VIII. RESULTS

A. Counting Results

The observed number of events in data is compared to the expected background in Fig. 2, as a function of jet multiplicity. Results are shown for the single and double b-tagging categories separately. Tables VI, VII and VIII show the composition of $W + 2$ jet data separately in each b-tagging category and in the central lepton and plug lepton regions, respectively.

The observed number of events in the data and the SM background expectations are consistent in each b-tagging category.

B. Limit on Higgs Boson Production Rate

We apply the neural network to the samples of simulated events and obtain the distributions of the network output for all the processes considered. After weighting their expected event yields, the resulting distributions are compared to the data observed in single and double b-tagging categories as shown in Fig. 3. We use a binned likelihood technique to fit the observed neural network distributions in three b-tagging categories to test for the presence of a WH signal. No excess over the background is observed. We therefore proceed to set an upper limit on the WH production cross section times $H \to b\bar{b}$ branching fraction.

	Central region	Plug region
Pretag Events	32242	5879
Mistag	107.1±9.38	28.47±3.30
$Wb\bar{b}$	215.6±92.34	43.09±12.33
$Wc\bar{c}$	167.0±62.14	33.37±9.55
$t\bar{t}$(6.7pb)	60.68±9.30	7.17±1.00
Single top(s-ch)	14.38±2.09	1.53±0.20
Single top(t-ch)	29.57±4.33	3.54±0.47
WW	15.45±1.91	3.00±0.20
WZ	7.59±0.81	1.62±0.09
ZZ	0.31±0.03	0.02±0.00
$Z->\tau\tau$	7.27±1.12	0.24±0.03
nonW QCD	184.7±33.04	18.34±5.54
Total Bkg	809.61±159.38	140.4±16.9
WH signal (120 GeV)	1.70±0.14	0.20±0.01
Observed Events	805	138

TABLE VI: Predicted sample composition and observed number of $W + 2$ jet events with exactly one SECVTX b-tag that passes the NN b-tagging filter.

The number of events in each bin follows the Poisson distribution

$$P_i(n_i, \mu_i) = \frac{\mu_i^{n_i} e^{-\mu_i}}{n_i!} \quad (i = 1, 2, \cdots, N_{\rm bin}), \tag{6}$$

where n_i, μ_i, and $N_{\rm bin}$ represent the number of observed events in the i-th bin, the expectation in the i-th bin, and the total number of bins. The Higgs production hypothesis is constructed by setting μ_i to $\mu_i = s_i + b_i$, where s_i and b_i are the number of signal and expected background events in the i-th bin. This quantity s_i can also be written as a product

$$s_i = \sigma(p\bar{p} \to W^{\pm}H) \cdot \mathcal{B}(H \to b\bar{b}) \cdot \epsilon_{WH} \cdot \int \mathcal{L}dt \cdot f_i^{WH}, \tag{7}$$

where f_i^{WH} is the fraction of the total signal which lies in the i-th bin. In this case, $\sigma(p\bar{p} \to W^{\pm}H) \cdot \mathcal{B}(H \to b\bar{b})$ is the variable to be extracted from data. An upper limit on the Higgs

	Central region	Plug region
Njet	2jet	
Pretag Events	32242	5879
Mistag	3.88±0.35	1.00±0.18
$Wb\bar{b}$	37.93±16.92	7.40±3.96
$Wc\bar{c}$	2.88±1.25	0.96±0.49
$t\bar{t}$(6.7pb)	19.05±2.92	2.14±0.34
Single top(s-ch)	6.90±1.00	0.69±0.10
Single top(t-ch)	1.60±0.23	0.22±0.04
WW	0.17±0.02	0.01±0.01
WZ	2.41±0.26	0.58±0.06
ZZ	0.06±0.01	0.00±0.00
$Z->\tau\tau$	0.25±0.04	0.00±0.00
nonW QCD	5.50±1.00	1.16±0.44
Total Bkg	80.62±18.75	14.18±4.03
WH signal (120 GeV)	0.85±0.10	0.09±0.01
Observed Events	83	11

TABLE VII: Predicted sample composition and observed number of $W+2$ jet events with at least two SECVTX b-tagged jets.

boson production cross section times branching fraction $\sigma(p\bar{p} \rightarrow W^{\pm}H) \cdot \mathcal{B}(H \rightarrow b\bar{b})$ is extracted by using a Bayesian procedure.

The likelihoods from the three b-tagging categories are multiplied together. The systematic uncertainties associated with the pretag acceptance, luminosity uncertainty, and uncertainty of the b-tagging efficiency scale factor are considered to be fully correlated between the three selection channels. Background uncertainties, specifically on the heavy-flavor fractions and b-tagging scale factor, are also completely correlated. The systematic uncertainties associated with the shape of network output are also studied and found to have a negligible impact on the final results. We assume an uniform prior probability for $\sigma \cdot \mathcal{B}$ and integrate the likelihood over all parameters except $\sigma \cdot \mathcal{B}$. A 95% confidence level upper limit on $\sigma \cdot \mathcal{B}$

	Central region	Plug region
Njet	2jet	
Pretag Events	32242	5879
Mistag	11.73±0.92	3.18±0.49
$Wb\bar{b}$	31.15±14.03	6.23±3.37
$Wc\bar{c}$	7.87±3.43	1.53±0.81
$t\bar{t}$(6.7pb)	15.56±2.39	1.79±0.31
Single top(s-ch)	5.14±0.75	0.51±0.08
Single top(t-ch)	1.87±0.27	0.24±0.04
WW	0.93±0.11	0.12±0.04
WZ	1.84±0.20	0.42±0.05
ZZ	0.08±0.01	0.01±0.00
$Z->\tau\tau$	1.29±0.20	0.01±0.00
nonW QCD	9.55±1.73	1.51±0.55
Total Bkg	86.99±17.99	15.54±3.56
WH signal (120 GeV)	0.60±0.07	0.06±0.01
Observed Events	90	13

TABLE VIII: Predicted sample composition and observed number of $W + 2$ jet events with one SECVTX plus Jet probability b-tagged jets.

is obtained by calculating the 95^{th} percentile of the resulting distributions.

To measure the expected sensitivity for this analysis, background-only pseudo-experiments are used to calculate an expected limit in the absence of Higgs boson production. Pseudo-data are generated by fluctuating the individual background estimates within total uncertainties. The expected limit is derived from the median of 95% confidence level upper limit of the one thousand pseudo-data.

The observed limits as a function of the Higgs boson mass are shown in Fig. 4 and Table IX, together with the expected limits determined from pseudo-experiments. We set 95% confidence level upper limit on the production cross section times branching fraction ranging from 1.2 to 1.1 pb or 7.5 to 101.9 times the Standard Model expectation for Higgs

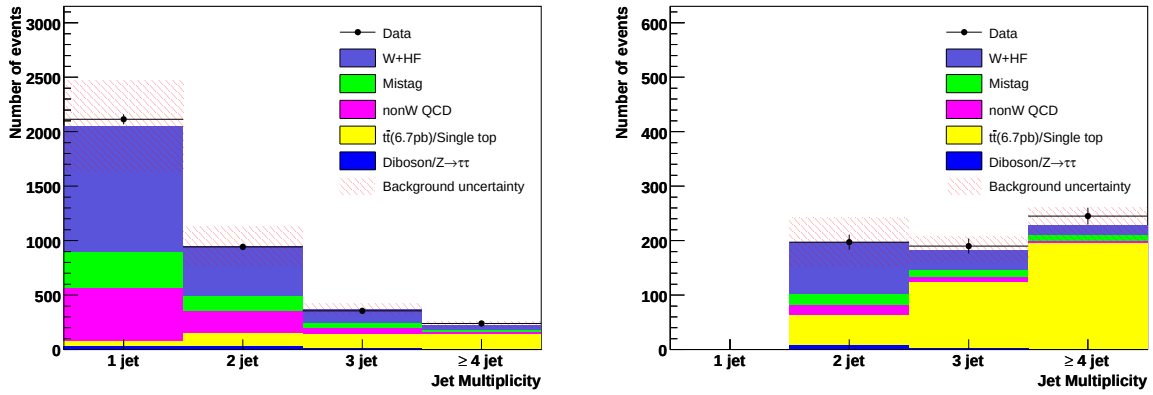

FIG. 2: Number of events as a function of jet multiplicity for events with exactly one SECVTX b-tag applying the NN b-tagging filter requirement (left) and for events with at least two SECVTX b-tagged jets or one SECVTX b-tagged jet plus one jet probability b-tagged jet (right).

Higgs Mass	Upper Limit (pb)		Upper Limit/SM	
GeV/c^2	Observed	Expected	Observed	Expected
110	1.2	1.2	7.5	7.8
115	1.2	1.1	9.0	8.7
120	1.1	1.1	10.2	10.5
130	1.1	0.9	17.9	15.2
140	1.2	0.8	40.1	28.7
150	1.1	0.8	101.9	70.9

TABLE IX: Observed and expected upper limits on $\sigma(p\bar{p} \to WH) \cdot \mathcal{B}(H \to b\bar{b})$ at 95 % C.L. compared to the SM production rate calculated at NNLO.

boson masses from 110 to 150 GeV/c^2, respectively. The search sensitivity is improved significantly with respect to previous searches, by about 60% more than the expectation from simple luminosity scaling. The main improvements are using jet probability b-tagging, a multivariate NN technique to further enhance sensitivity to the signal, and increasing the acceptance for signal events by including leptons in the forward region of the detector.

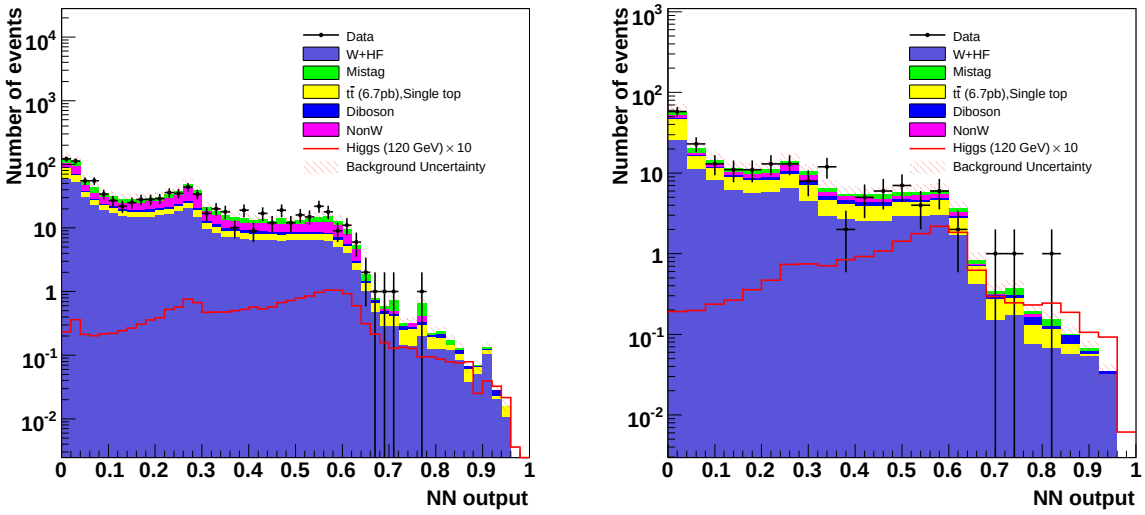

FIG. 3: Neural Network output distribution in W+2 jets events for exactly one SECVTX b-tagged jet that passes the NN b-tagging filter (left) and events for ST+ST and ST+JP double b-tagging categories (right). The contributions of the various background sources from the central plus plug region are shown in histograms while the hatched box represents the background uncertainty.

IX. CONCLUSIONS

We have presented a search for the standard model Higgs boson in the $\ell\nu b\bar{b}$ final state expected from WH production at CDF. The candidate events are separated into three b-tagging categories and optimized for this search. In addition, we have increased the signal acceptance by including electrons in the forward region of the detector and used a neural network discriminant to further enhance sensitivity to the signal. These improvements, along with a dataset of $1.9\,\mathrm{fb}^{-1}$, allow us to set a 95% confidence level upper limit on the production cross section times branching fraction that ranges from 1.2 to 1.1 pb or 7.5 to 101.9 times the Standard Model expectation for Higgs boson masses spanning 110 to $150\,\mathrm{GeV}/c^2$, respectively.

Acknowledgments

We thank the Fermilab staff and the technical staffs of the participating institutions for their vital contributions. This work was supported by the U.S. Department of Energy and

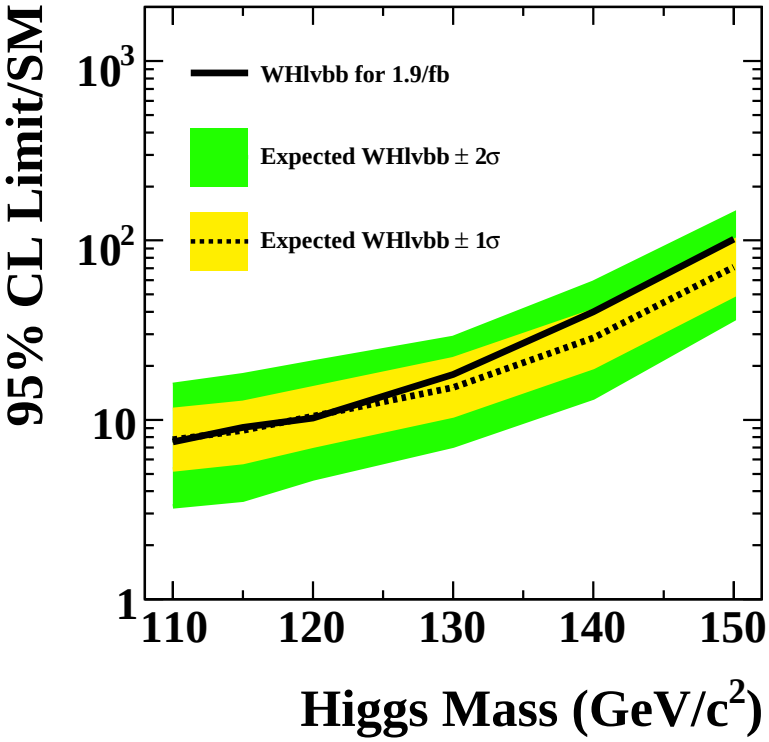

FIG. 4: The observed (solid) and expected (dash) 95% confidence level upper limit on $\sigma(p\bar{p} \rightarrow WH) \cdot \mathcal{B}(H \rightarrow b\bar{b})$ relative to the SM expectations with an integrated luminosity of 1.9 fb^{-1} obtained from the likelihood combined central and plug lepton region with three b-tagging categories.

National Science Foundation; the Italian Istituto Nazionale di Fisica Nucleare; the Ministry of Education, Culture, Sports, Science and Technology of Japan; the Natural Sciences and Engineering Research Council of Canada; the National Science Council of the Republic of China; the Swiss National Science Foundation; the A.P. Sloan Foundation; the Bundesministerium für Bildung und Forschung, Germany; the Korean Science and Engineering Foundation and the Korean Research Foundation; the Particle Physics and Astronomy Research Council and the Royal Society, UK; the Institut National de Physique Nucleaire et Physique des Particules/CNRS; the Russian Foundation for Basic Research; the Comisión Interministerial de Ciencia y Tecnología, Spain; the European Community's Human Poten-

tial Programme under contract HPRN-CT-2002-00292; and the Academy of Finland.

---

[1] P. W. Higgs, Phys. Rev. Lett. **13**, 508 (1964).

[2] R. Barate et al. (ALEPH, DELPHI, L3, and OPAL collaborations and the LEP Working Group for Higgs boson searches), Phys. Lett. **B565**, 61 (2003), hep-ex/0306033.

[3] J. Alcaraz et al. (ALEPH, DELPHI, L3, and OPAL collaborations and the LEP Electroweak Working Group), Tech. Rep. CERN-PH-EP-2006-042 (2006), hep-ex/0612034.

[4] T. Han and S. Willenbrock, Phys. Lett. **B273**, 167 (1991).

[5] A. Djouadi, J. Kalinowski, and M. Spira, Comput. Phys. Commun. **108**, 56 (1998), hep-ph/9704448.

[6] A. Abulencia et al. (CDF collaboration), Phys. Rev. **D75**, 012010 (2007), hep-ex/0612015.

[7] T. Aaltonen et al. (CDF), Phys. Rev. Lett. **100**, 041801 (2008), 0710.4363.

[8] T. Aaltonen et al. (CDF), Phys. Rev. **D78**, 032008 (2008), 0803.3493.

[9] V. M. Abazov et al. (D0 collaboration), Phys. Lett. B **663**, 26 (2008), hep-ex/0712.0598.

[10] D. Acosta et al. (CDF collaboration), Phys. Rev. **D71**, 032001 (2005), hep-ex/0412071.

[11] L. Balka et al., Nucl. Instrum. Methods **A267**, 272 (1988).

[12] S. Bertolucci et al., Nucl. Instrum. Methods **A267**, 301 (1988).

[13] M. G. Albrow et al., Nucl. Instrum. Methods **A480**, 524 (2002).

[14] F. Abe et al. (CDF collaboration), Phys. Rev. **D45**, 1448 (1992).

[15] A. Bhatti et al., Nucl. Instrum. Methods **A566**, 375 (2006), hep-ex/0510047.

[16] G. Ascoli et al., Nucl. Instrum. Methods **A268**, 33 (1988).

[17] T. Dorigo (CDF collaboration), Nucl. Instrum. Methods **A461**, 560 (2001).

[18] E. J. Thomson et al., IEEE Trans. Nucl. Sci. **49**, 1063 (2002).

[19] D. Acosta et al. (CDF collaboration), Phys. Rev. Lett. **94**, 091803 (2005), hep-ex/0406078.

[20] D. Acosta et al. (CDF collaboration), Phys. Rev. **D71**, 052003 (2005), hep-ex/0410041.

[21] A. Abulencia et al. (CDF collaboration), Phys. Rev. Lett. **97**, 082004 (2006).

[22] C. Peterson, T. Rögnvaldsson, and L. Lönnblad, Comput. Phys. Commun. **81**, 185 (1994).

[23] A. Abulencia et al. (CDF collaboration), Phys. Rev. **D74**, 072006 (2006), hep-ex/0607035.

[24] A. Abulencia et al. (CDF collaboration), Phys. Rev. Lett. **97**, 082004 (2006), hep-ex/0606017.

[25] M. L. Mangano, M. Moretti, F. Piccinini, R. Pittau, and A. D. Polosa, J. High Energy Phys.

07, 001 (2003), hep-ph/0206293.

[26] G. Corcella et al. (2001), hep-ph/0201201.

[27] J. Campbell and R. K. Ellis, Phys. Rev. **D65**, 113007 (2002), hep-ph/0202176.

[28] M. Cacciari, S. Frixione, M. L. Mangano, P. Nason, and G. Ridolfi, J. High Energy Phys. **04**, 068 (2004), hep-ph/0303085.

[29] B. W. Harris, E. Laenen, L. Phaf, Z. Sullivan, and S. Weinzierl, Phys. Rev. **D66**, 054024 (2002), hep-ph/0207055.

[30] T. Sjöstrand et al., Comput. Phys. Commun. **135**, 238 (2001), hep-ph/0010017.

[31] A. Abulencia et al. (CDF collaboration), Phys. Rev. **D73**, 032003 (2006), hep-ex/0510048.

[32] J. Pumplin et al., J. High Energy Phys. **07**, 012 (2002), hep-ph/0201195.